Triboelectric Nanogenerator with Enhanced Performance via an Optimized Low Permittivity Substrate

Gunabo Min, Libu Manjakkal, Daniel M. Mulvihill and Ravinder S. Dahiya

***Abstract*— With electrical power generated from mechanical contact, triboelectric nanogenerators (TENGs) offer a promising route to realizing self-powered sensors. For effective usage, it is important to improve their limited power range (0.1-100 mW/cm^2) and this can be achieved by optimizing the output performance. Among the factors that confer higher performance are materials with a strong triboelectric effect together with low permittivity, but it is challenging to optimize both within a single material. This paper presents a solution to this challenge by optimizing a low permittivity substrate beneath the tribo-contact layer. Results are simulated over a range of substrate permittivities. The open circuit voltage is found to increase by a factor of 1.6 in moving from PVDF to the lower permittivity PTFE. Two TENG devices have been fabricated with 100μm PET and PTFE substrates to compare performance. The experiments confirm that lowering the substrate dielectric constant (i.e. PET to PTFE) raises the open circuit voltage in line with simulation predictions.**

***Index Terms*— Triboelectric nanogenerator; Self-powered Sensors; Simulation; Permittivity; Dielectric**

I. Introduction

Self-powered or energy autonomous sensors are key to the acceptance of next generation wearable devices for healthcare [1], robotics [2], environment monitoring [3] and internet of things (IoT) applications [4] etc. As a result, energy harvesting through various mechanisms such as triboelectric [5], piezoelectric [6], thermoelectric [7] and photovoltaics [2] has been widely explored. Among these, triboelectric nanogenerators (TENGs) are most promising for self-powered applications, owing to attractive features such as high-efficiency, flexibility, light-weight, portability, and low-cost. For these reasons, TENGs are being developed as a potential power supply source for a variety of wearable, implantable and flexible systems such as micro/nano-sensors [8,9], robotics [10], health monitoring [11-15] and tribotronic transistors [16-18]. It is also possible to use this method to generate electricity for wearable systems from daily movements such as walking, running and pulse beating [20-22] etc.

The power generation of TENGs depends on the principle of triboelectrification, dielectric material capacitance and electrostatic induction. The tribo-charge density, which is key to power generation, as well as, driving charge flow in TENGs, (Fig. 1) depends on the strength of the triboelectric effect generated by a particular interface pair [23-26]. The open circuit voltage in TENGs can be obtained by using a distance-dependent electric field model [26]. As per this model, the open circuit voltage can be optimized by increasing the intensity of electric field generated by the tribo-charges. According to Gauss's law [27], the electric field strength increases with increasing charge density and decreasing permittivity of the medium. Hence, it is clear that materials offering both low permittivity within the tribo-layer and a strong triboelectric effect would lead to an optimum outcome. However, it is difficult to find a material pair capable of conferring both properties. For instance, polyvinylidene difluoride (PVDF) is an intensely negative triboelectric material [23] (due to the high work function of the fluorine atoms [28-31]), but it has high permittivity.

Optimization is important considering the current gap between the limited power (~0.1- 100 mW/cm^2) available from TENGs [34] and the power needed to develop self-powered sensors and electronics (8.44- 107mW/m^2) [35]. In this regard, this paper presents a study on optimizing a low permittivity substrate (yellow layer in Fig. 1) below the tribo-contact surface so that gains from both strong triboelectric effect and low permittivity can be harnessed in a single device architecture. This paper extends the preliminary results presented at IEEE Sensors 2018 [36], where we presented simulation based study to investigate the effects of varying substrate relative permittivity upon TENG outputs such as open circuit voltage, short circuit charge density and short circuit current density. In

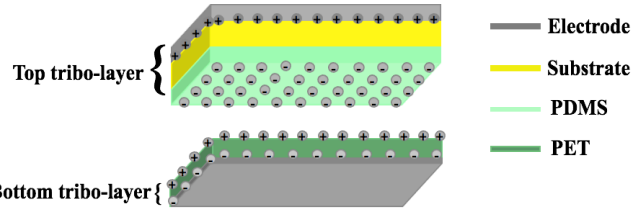

Fig. 1. Contact mode 'TENG' with low permittivity 'substrate' (in yellow).

An earlier version of this paper was presented at IEEE Sensors Conference, 2018 and published in its proceedings [DOI: 10.1109/ICSENS.2018.8589631 https://ieeexplore.ieee.org/abstract/document/8589631]

This work was supported in part by the EPSRC Engineering Fellowship for Growth (EP/M002527/1 and EP/R029644/1).

G. Min, L. Manjakkal and R.S. Dahiya are with Bendable Electronics and Sensing Technologies (BEST) Group, University of Glasgow, G12 8QQ, UK

G. Min and D.M. Mulvihill are with the Materials and Manufacturing Research Group, University of Glasgow, G12 8QQ, UK (e-mail: daniel.mulvihill@glasgow.ac.uk).

(Correspondence to: Ravinder.Dahiya@glasgow.ac.uk)

addition to further in-depth simulation, here we also test two TENG devices fabricated with polyethylene terephthalate (PET) and polytetrafluoroethylene (PTFE) substrates to verify the simulation results. In order to assess the influence of substrate permittivity *only*, the tribo-contact materials are fixed as PET and PDMS films (see Fig. 1) in both the simulations and experiments. Therefore, the tribo-charge density of the devices can be considered constant. Other factors affecting the output parameters where also fixed to enable comparison including separation distance, frequency and applied force.

The remainder of the paper is organized as follows: the principle of operation of the contact mode TENG is explained in Section II. The simulation and fabrication details are outlined in Section III and the key results with comparisons between simulation and experiments are discussed in Section IV. Finally, the key outcomes are summarized in Section V.

II. Working of Contact Mode TENG

The tribo-charges are the power source which drives the TENGs to produce the free charges on the electrodes. In contact-separation TENGs (CS-TENGs), coupling of triboelectrification and electrostatic induction [23] define the operating principle. The transfer of opposite and equal tribo-charges occurs on each contact surface, owing to the difference in the triboelectrification property of the contacting materials [24]. The working principle applying to the open circuit voltage and short circuit current condition for a CS-TENG is shown schematically in Fig. 2. The output performance of a TENG is actually dependent upon many factors, including surface roughness, thicknesses, separation distance, contact material properties, etc, but our primary concern in this work is with substrate dialectric constant. The open circuit voltage and short circuit current are the significant parameters for presenting the

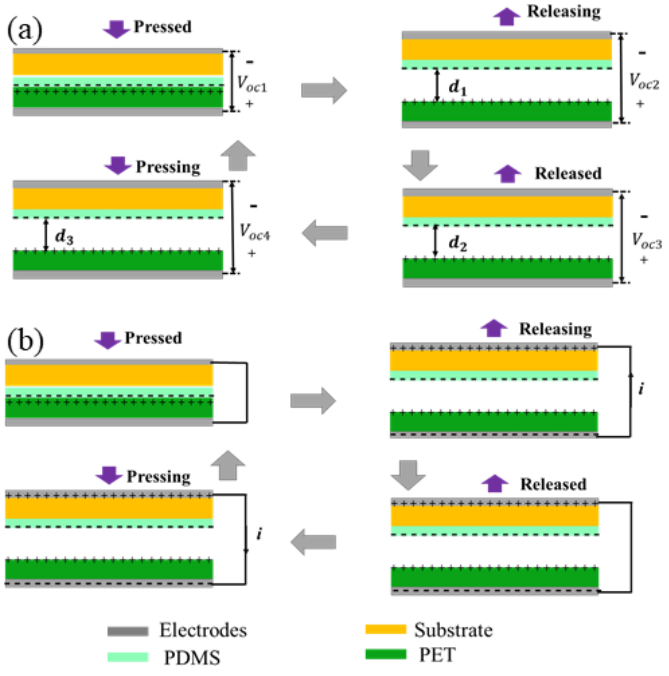

Fig. 2: Working principle of contact-mode triboelectric nanogenerators: (a) open circuit voltage (b) short circuit current.

performance of CS-TENGs [23-26]. There is no free charge on the two electrodes for the open circuit configuration in Fig. 2(a) [23]. The open circuit voltage is created by the difference in potential between the electrodes as separation occurs. Simultaneously, these built-in electric fields cause the polarization of the dielectric material and produce the induced charges on the electrodes [25]. In short circuit mode, the charge is transferred from one electrode to the other. Therein, the separation distance between the interface pairs is one of most important parameters. Different open circuit voltages will be developed with different separations [24,26]. The building of potential on the electrodes is also related to the intensity of the internal electric field of TENGs. This depends on both the tribo-charge density σ_T and the permittivity ε as:

$$E = \frac{\sigma_T}{2\varepsilon} \tag{1}$$

The tribo-layers of CS-TENGs can be thought of as equivalent to two capacitors (Fig. 1) and the intensity of the electric field can be improved with low permittivity tribo-layer materials [26].

The open circuit voltage (V_{oc}) is related to tribo-charge density, contact area and the capacitance of tribo-layers [24] according to:

$$V_{oc} = \frac{\sigma_T A}{C_o} \tag{2}$$

Where, the σ_T is the tribo-charge density, A is the contact area and C_o is the capacitance of the tribo-layer. Eq. 2 shows that there are no free charges on the electrodes at open circuit stage. However, there should be the energy transformation in the tribo-layers. Thus, the dielectric materials in the tribo-layers are polarized at the open circuit stage. Due to the capacitance property, this can be calculated as [37]

$$C_o = \frac{\varepsilon_r \varepsilon_0 A}{d} \tag{3}$$

Where, ε_r and ε_0 are the permittivity of the dielectric material and of vacuum respectively and d is the distance between the two electrodes. The range of the variation for the distance between tribo-charges and electrode varies from the thickness of a tribo-layer to the sum of tribo-layer thicknesses and separation distance. Simultaneously, because the potential of each electrode is affected by the tribo-charges on two contact surfaces (see Fig. 2(a)), the open circuit voltage can be investigated by the distance-dependent model [26] as:

$$V_{oc} = \frac{\sigma_T}{\pi\varepsilon_1}\left[\int_{d_1}^{d_1+z} f(x)dx\right] - \frac{-\sigma_T}{\pi\varepsilon_2}\left[\int_{d_2}^{d_2+z} f(x)dx\right] \tag{4}$$

Where, z is the separation distance between two contact surfaces, d_1 and d_2 are the thickness of the tribo-layers and $f(x)$ is the distance variation function. Therefore, Eq. 4 shows how a low permittivity tribo-layer can increase the open circuit voltage. The potential of the electrodes is also influenced by the induced free charges on the electrodes at the short circuit stage and the free charge density and short circuit current density can be calculated by putting the differential potential between the

two electrodes equal to zero [24, 26].

III. Simulation and Fabrication

A. Simulation

Using the distance-dependent electric field model of CS-TENGs [26, 38], the open circuit voltage (Eq. 4) and short circuit current was simulated (using MATLAB) for different substrate relative permittivities. The simulated TENG consists of two contacting layers which can be thought of as a parallel plate capacitor (Fig. 1). The 'top tribo-layer' is comprised of the tribo-contact material, the substrate and the electrode while the 'bottom tribo-layer' comprises just the partner tribo-contact material and its electrode. The interface pair (i.e. the tribo-contact material pair) was nominally selected as PDMS and PET (as in Fig. 1) to allow direct comparison with results from [26]. Accordingly, a tribo-charge density of 40.7 μC/m^2 was used as in [26]. First, TENG operation was simulated for a selection of substrate materials and an optimum material was chosen based on optimum permittivity. The total equivalent permittivity of the top tribo-layer can be calculated by the parallel plate capacitor model. The capacitance of the substrate layer (in the top tribo-layer) is given by $C = \varepsilon A / d$ [39], where C is capacitance, ε is permittivity, d is thickness of medium and A is the in-plane area. If the capacitance of the top layer is supposed as two dielectrics in one capacitor, the equivalent capacitance of the two materials comprising the top tribo-layer can be presented as:

$$\frac{1}{C_{eq}} = \frac{1}{C_1} + \frac{1}{C_2} \tag{5}$$

Where, C_1 and C_2 are the capacitances of PDMS and the substrate respectively. Combining Eq. 5 and the formula for capacitance above, the total relative permittivity of the 'top tribo-layer' can be calculated by [36] as:

$$\varepsilon_{r,eq} = \frac{\varepsilon_{r,PDMS}\varepsilon_{r,Substrate}(d_{PDMS}+d_{substrate})}{d_{PDMS}\varepsilon_{r,Substrate}+d_{Substrate}\varepsilon_{r,PDMS}} \tag{6}$$

Where, the $\varepsilon_{r,PDMS}$ and $\varepsilon_{r,Substrate}$ are the relative permittivity values of PDMS and the substrate, respectively and d_{PDMS} and $d_{substrate}$ are the thicknesses of PDMS and the substrate film (the 'yellow' layer in Fig. 1). Using the relative permittivity for PDMS (Table I) together with the substrate relative permittivity values in Table II (first column), the equivalent relative permittivity of the top tribo-layer was calculated using Eq. 6 for a range of substrate materials (PTFE, PET, Paper, Bakelite, Neoprene rubber and PVDF). These are listed as the second column in Table II. The third column in Table II gives the equivalent absolute permittivity of the 'top tribo-layer'. These materials represent a relatively wide range of permittivity values. Therefore, the relationship between substrate permittivity and TENG output (i.e. open circuit voltage, short circuit charge density and short circuit current density) can be summarized by simulating TENGs having these substrate materials. This essentially allows determination of an optimum substrate material. In the first part of the simulation work, the effect of substrate material relative permittivity on TENG output performance was studied using the same dimensions as in previous literature [26], including the nominal contact area of 5cm×5cm and the thickness of the interface pairs (PDMS and PET) of $20\mu m$ and $200\mu m$. This was done to allow direct comparison with the result in [26] where a PET substrate was used. Subsequently, the thicknesses of the PDMS and PET were altered to $20\mu m$ and $127\mu m$ and the nominal contact area was altered to 2cm×2cm (see Table III) in order to match the devices fabricated in this work. Moreover, the thickness of the substrates was fixed at $100\mu m$. The relationship between substrate permittivity and TENG output was simulated by these parameters to compare the simulation and experimental results. Note, that the substrate is implanted under the negative triboelectric interface (PDMS). Based on these parameters, the open circuit voltage, short circuit current and charge have been simulated and results are discussed in section IV.

Table I. Parameters for 'top tribo-layer'.

Substrate (PTFE, PET, Paper, Bakelite, Neoprene rubber, PVDF)	Contact Material (PDMS)
Thickness = $\mathbf{100\mu m}$	Thickness = $20\mu m$
Relative Permittivity ($\boldsymbol{\varepsilon_{r1}}$) varying (depending on type of substrate)	Relative Permittivity ($\varepsilon_{r2} = 2.7$)
Size: $\mathbf{2cm \times 2cm}$	Size: 2cm × 2cm

Table II. Substrate relative material permittivity ε_r, 'top tribo-layer' relative equivalent permittivities $\varepsilon_{r,eq}$ and 'top tribo-layer' absolute equivalent permittivities ε_{eq}.

Substrate Materials	ε_r of substrate materials	$\varepsilon_{r,eq}$ of top tribo-layer	ε_{eq} of top tribo-layer × 10^{-12}F/m
PTFE (Teflon)	2.1	2.2	19.3
PET	3.3	3.2	28.2
Paper	3.7	3.5	30.9
Bakelite	4.9	4.3	38.3
Neoprene Rubber	6.7	5.4	47.7
PVDF	7.5	5.8	51.3

B. Fabrication

For the experimental aspect of the work, two types of devices were fabricated based on two substrate materials having sufficiently different permittivity values (PTFE and PET - see Table III for comparison). The overall approach to device

Table III: Comparison of fabricated TENG devices and test parameters

Device 1	Device 2
Sample Size = 2 cm × 2cm	Sample Size = 2 cm × 2cm
Negative Contact Material – PDMS ($20\mu m$ thickness, $\varepsilon_{PDMS} = 2.7$)	Negative Contact Material – PDMS ($20\mu m$ thickness, $\varepsilon_{PDMS} = 2.7$)
Positive Contact Material – ITO coated PET film ($127\mu m$ thickness, $\varepsilon_{PET} = 3.3$)	Positive Contact Material – ITO coated PET film ($127\mu m$ thickness, $\varepsilon_{PET} = 3.3$)
Substrate Material – PET film ($100\mu m$ thickness, $\varepsilon_{PET} = 3.3$)	Substrate Material – PTFE film ($100\mu m$ thickness, $\varepsilon_{PTFE} = 2.1$)
4Hz Operation frequency	4Hz Operation frequency
8N applied force	8N applied force
1mm separation distance	1mm separation distance

structure and fabrication is somewhat similar to that employed by Dharmasena *et al*. [26] with some differences. The bottom half of the TENG was fabricated simply as ITO coated PET film (sheet resistivity = 60Ω/sq, thickness 0.127mm, Sigma Aldrich, UK). The top half consisted of PDMS, the substrate material (either PET or PTFE) and a gold coating as the electrode. PDMS is the negative contact layer and PET is the positive

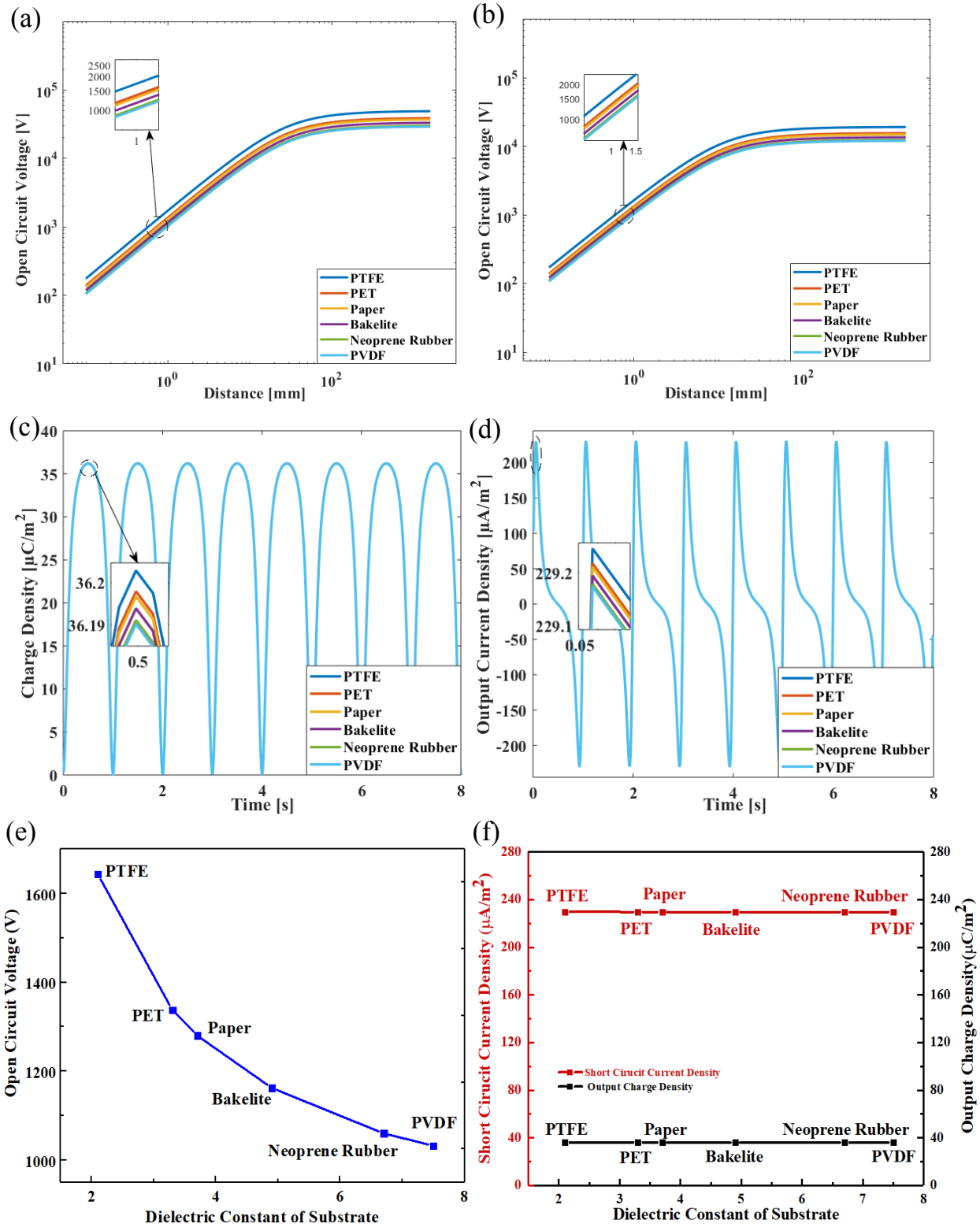

Fig. 3: Simulation results: (a) Open circuit voltage vs separation distance with 5cm×5cm areas and 200μm thickness substrate, (b) Open circuit voltage vs separation distance with 2cm×2cm areas and 100μm thickness substrate, (c) Short circuit charge density vs time, and (d) Short circuit current density vs time with substrate materials having a range of permittivity values (at 1mm separation distance for c and d), (e)–(f) Open circuit voltage, short circuit current density and short circuit charge density versus relative permittivity for different substrate materials (at 1mm separation).

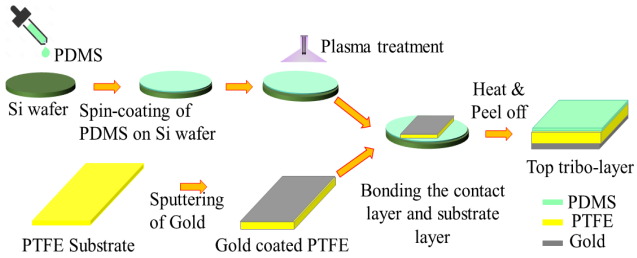

Fig. 4: Fabrication steps for the 'of top tribo-layer'

contact layer. To create the PDMS layer, PDMS cross-linker was mixed with its elastomer by a 1:10 ratio and degassed under vacuum for 45 min. Subsequently, the PDMS was spin-coated on a silicon wafer symmetrically at 3800 rpm for 60 seconds to obtain a 20 μm thickness. In this experiment, the negative contact material (PDMS) and the positive contact layer material (PET) were fixed in order to ensure the same tribo-charge density generation for each device. A substrate sheet (100 µm thickness of either PET or PTFE) with 2cm×2cm size was attached on the pervious PDMS layer and cured at 70℃ for 2 hrs. Finally, the gold film was deposited. The fabrication steps for the top triboelectric layer are shown Fig. 4. A layer of Kapton tape was required on each electrode for sufficient isolation. The mechanical energy supply for the TENGs was supplied by an oscillating force (maximum 8 N with frequency 4 Hz) using a TIRA shaker. The separation distance was fixed at 1mm and the open circuit voltage was recorded by an oscilloscope (KETSIGHT, MSO-X 4154A). The oscilloscope was connected with a voltage separation circuit comprising a 1 GOhm and a 10 MOhm resistor as shown schematically in Fig. 5. This was done to ensure that the impedance of the voltage meter setup was much larger than the TENG internal impedance. The short circuit current was measured using a digital multimeter (Keysight Technologies 34460A, 6 1/2-digit, basic Truevolt DMM) and logged using LabVIEW.

IV. Results and Discussion

A. Simulation Results

Fig. 2(a-b) illustrates the cycle of interaction of the layered TENG, while Fig. 3(a) presents the device's outputs (open circuit voltage vs separation distance) for device dimensions of 5cm×5cm. Fig. 3(b-d) reports the device output (open circuit voltage vs separation distance, short circuit charge density vs time and short circuit current density vs time) for a device

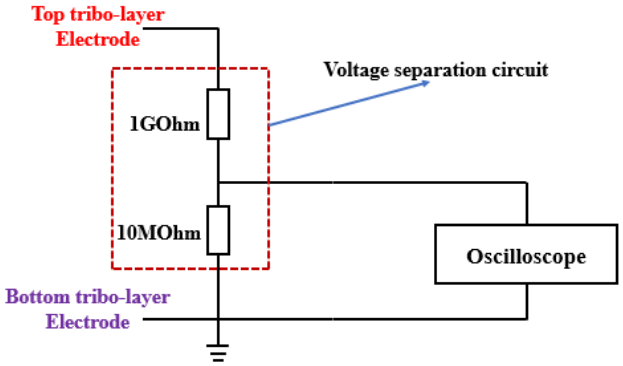

Fig. 5: Schematic of the voltage separation circuit.

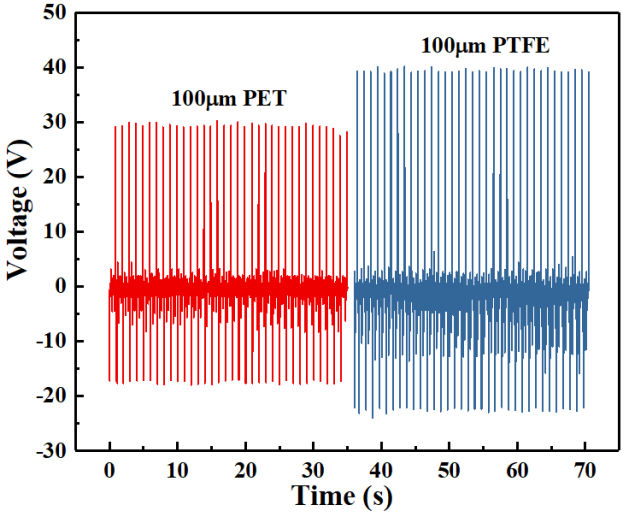

Fig. 6: Comparison of open circuit voltage signals for the devices with PTFE and PET substrates.

having the same dimensions as the experimental devices (i.e. 2 cm x 2 cm). Fig. 3(e-f) then plots these outputs (2 cm x 2 cm area) explicitly against relative permittivity. Note, the results in Fig. 3(c-f) are for a 1 mm separation distance. It is clear from Fig. 3(a) that open circuit voltage increases significantly as the relative permittivity of the 'top tribo-layer' is reduced. Unsurprisingly, the trend in Figs. 3(a) and 3(b) is similar as only the device area and layer thicknesses have changed. In Fig. 3(e), the open circuit voltage increases from 1032 V to 1643 V (i.e. 1.6 times), when the substrate material changes from PVDF to PTFE (i.e. relative permittivity of substrate reduced from 7.5 to 2.1). The improvement with PTFE is 1.23 times the output reported in [26] with PET (ε_r = 3.3) as the substrate material (the result from [26] is identical to the Orange line in Fig. 3(a)). Hence, open circuit voltage can be enhanced by embedding a substrate with lower relative permittivity than the original triboelectric contact material to reduce the relative equivalent permittivity of the overall top triboelectric layer in Fig. 1. Although Fig. 3(c-d) shows short circuit charge and current density declining somewhat with increasing relative permittivity, Fig. 3(f) shows that the change is insignificant relative to the magnitudes of these outputs. Over the range of relative permittivity, they are approximately fixed at about 36.2 $\mu C/m^2$ and 229.2 $\mu A/m^2$ respectively. Hence, by choosing PTFE as the optimum substrate material, we can obtain useful increases in open circuit voltage while not affecting current and charge density very much. In summary, the simulation results have indicated that open circuit voltage can be significantly improved, while short circuit charge density and short circuit current density are only very slightly increased by implanting a low permittivity material under the negative triboelectric interface.

B. Experimental Results

In order to provide a preliminary check on the validity of the simulation predictions, two materials from Table II (PET and PTFE – the best performing substrate materials in Fig. 3(e)) were chosen as the substrate material and two corresponding TENG devices were fabricated (described above) and tested. The devices were fabricated identically – the only difference being the relative permittivity of the substrate material reduces

from 3.3 to 2.1 in going from a PET to PTFE substrate. Identical interface materials ensure that both devices generate the same tribo-charge density. Test conditions were also identical for both devices: a frequency of 4 Hz, a max load of 8 N and a 1 mm separation distance. The substrate thickness was 100 μm for both devices. A 5 min pre-charge time was employed before each set of measurements to ensure equilibrium of tribo-charge generation. Table III summarises the device and test specifications. Fig. 6 plots the output open circuit voltage signal from both devices. The max output voltage increased from 29.5 to 39.4 V (i.e. 1.3 times) and the peak-to-peak value from 46.5 to 61.4 V (i.e. 1.3 times). These increases are very much in line with the simulation prediction from Fig. 3(e) where the simulated open circuit voltage increased by 1.3 times between PET and PTFE. Note, that the voltage magnitudes between simulation (Fig. 3e) and experiment (Fig. 6) are quite different however. A key reason for this is likely to be because the simulation results are based on a prefect contact interface; whereas, the amount of 'real contact area' in the experimental device (at these loads) is likely to be only a fraction of the nominal contact area. A lower experimental 'real contact area' would be likely to generate a reduced tribo-charge density at the interface and therefore, a reduced open circuit voltage output. Nevertheless, contrasting the relative voltage increase represents a valid comparison and results suggest that the experimental check is in-line with the simulation prediction (as both predict an increase in open circuit voltage of roughly 1.3 for the move from PET to PTFE). Finally, the experimental results showed no appreciable difference in short circuit current density in moving from PET to PTFE substrates as predicted by the simulation result in Fig. 3(f).

V. Conclusions

Materials with strong triboelectric effect and low permittivity are among the requirements for improving triboelectric nanogenerator (TENG) performance. These features are not always possible in the same material, so this paper outlines the idea of optimising a low permittivity substrate material underneath the tribo-contact layer so that both optimum triboelectric effect and low permittivity can be incorporated in the same TENG. Results (simulated using a distance-dependent electric field model) show that open circuit voltage increases with reducing substrate permittivity. Going from PVDF (ε_r =7.5) to PTFE (ε_r=2.1), open circuit voltage increased by a factor of 1.6. Therefore, PTFE was selected as a suitable substrate material. Therefore, simulation results show that low permittivity can be used to boast TENG performance. A preliminary check on the simulation results was provided by fabricating and testing two TENG devices having different substrate permittivity values. PET and PTFE substrates of 100 μm thickness were incorporated in otherwise identical devices. In moving from PET to PTFE substrates (ε_r = 3.3 to ε_r=2.1), the experiments predicted almost the same increase in open circuit voltage as the simulations (roughly 1.3 times). Experiments also confirmed little increase in short circuit current density with substrate permittivity as predicted by the simulations. The conclusion is that low permittivity substrates can be used to enhance the open circuit voltage of TENGs. Current work is concentrating on looking at this effect over a wider range of substrate materials. In future, we will focus on demonstrating the further significant gains predicted by further reducing the substrate thickness. Finally, TENGs are currently being considered as a viable autonomous energy supply source for a host of self-powered sensor technologies and the advances discussed here in terms of enhancing output will be directly useful in those sensor applications.

References

[1] Y. Cheng et al., "A stretchable fiber nanogenerator for versatile mechanical energy harvesting and self-powered full-range personal healthcare monitoring", *Nano Energy*, vol. 41, pp. 511-518, 2017.

[2] C. García Núñez, L. Manjakkal and R. Dahiya, "Energy autonomous electronic skin", *NPJ Flex Electron*, vol. 3, no. 1, 2019.

[3] L. Manjakkal, C. Núñez, W. Dang and R. Dahiya, "Flexible self-charging supercapacitor based on graphene-Ag-3D graphene foam electrodes", *Nano Energy*, vol. 51, pp. 604-612, 2018.

[4] A. Adila, A. Husam and G. Husi, "Towards the self-powered Internet of Things (IoT) by energy harvesting: Trends and technologies for green IoT", in *2018 2nd International Symposium on Small-scale Intelligent Manufacturing Systems (SIMS)*, April 2018, PP.1-5.

[5] F.-R. Fan, Z. Q. Tian and Z. L. Wang, "Flexible triboelectric generator," *Nano energy*, vol. 1, no. 2, pp. 328-334, 2012.

[6] E. S. Hosseini, L. Manjakkal, R. Dahiya, "Bio-organic Glycine based Flexible Piezoelectric Stress Sensor for Wound Monitoring," in *Proc. IEEE Sensors 2018*, Oct 2018, N. Delhi, India.

[7] S. Khan, R. S. Dahiya, and L. Lorenzelli, "Flexible thermoelectric generator based on transfer printed Si microwires," presented at the 44th Eur. Solid State Device Res. Conf. (ESSDERC), Venice, Italy, 2014, pp. 86–89

[8] Y. Wu et al., "A Self-Powered Triboelectric Nanosensor for PH Detection", *J. Nanomater*, vol. 2016, pp. 1-6, 2016.

[9] A. Ahmed, Z. Saadatnia, I. Hassan, Y. Zi, Y. Xi, X. He, J. Zu, Z. L. Wang, Self-Powered Wireless Sensor Node Enabled by a Duck- Shaped Triboelectric Nanogenerator for Harvesting Water Wave Energy. *Adv. Energy Mater*. 2017, 7, 1601705.

[10] T. Bu et al., "Stretchable Triboelectric-Photonic Smart Skin for Tactile and Gesture Sensing", *Adv. Mater*, vol. 30, p. 1800066, 2018.

[11] Tang et al., "Whirligig-inspired triboelectric nanogenerator with ultrahigh specific output as reliable portable instant power supply for personal health monitoring devices", *Nano Energy*, vol. 47, pp. 74-80, 2018.

[12] Z. Lin et al., "Triboelectric Nanogenerator Enabled Body Sensor Network for Self-Powered Human Heart-Rate Monitoring", *ACS Nano*, vol. 11, no. 9, pp. 8830-8837, 2017.

[13] X. Ding, H. Cao, X. Zhang, M. Li and Y. Liu, "Large Scale Triboelectric Nanogenerator and Self-Powered Flexible Sensor for Human Sleep Monitoring", *Sensors*, vol. 18, p. 1713, 2018.

[14] Z. Lin et al., "A Triboelectric Nanogenerator-Based Smart Insole for Multifunctional Gait Monitoring", *Adv. Mater. Technol*, vol. 4, p. 1800360, 2018.

[15] Q. Zheng et al., "In Vivo Self-Powered Wireless Cardiac Monitoring via Implantable Triboelectric Nanogenerator", *ACS Nano*, vol. 10, no. 7, pp. 6510-6518, 2016.

[16] Y. Liu, S. Niu and Z. Wang, "Theory of Tribotronics", *Adv. Electron. Mater*, vol. 1, no. 9, p. 1500124, 2015.

[17] T. Zhou, Z. Yang, Y. Pang, L. Xu, C. Zhang and Z. Wang, "Tribotronic Tuning Diode for Active Analog Signal Modulation", *ACS Nano*, vol. 11, no. 1, pp. 882-888, 2016.

[18] Y. Pang et al., "Flexible transparent tribotronic transistor for active modulation of conventional electronics", *Nano Energy*, vol. 31, pp. 533-540, 2017.

[19] S. Wang, L. Lin, and Z. L. Wang, "Triboelectric nanogenerators as self-powered active sensors," *Nano Energy*, vol. 11, pp. 436-462, 2015.

[20] J. Xiong et al., "Skin-touch-actuated textile-based triboelectric nanogenerator with black phosphorus for durable biomechanical energy harvesting", *Nat. Commun*, vol. 9, no. 1, 2018.

[21] X. Cui et al., "Pulse sensor based on single-electrode triboelectric nanogenerator", *Sens. Actuator A-Phys*, vol. 280, pp. 326-331, 2018.

[22] Li, Z., Shen, J., Abdalla, I., Yu, J. and Ding, B. Nanofibrous membrane constructed wearable triboelectric nanogenerator for high performance biomechanical energy harvesting. *Nano Energy*, 36, pp.341-348, 2017.
[23] Z. Wang, L.Lin, J.Chen, S.Niu and Y.Zi, *Triboelectric nanogenerators*, Switzerland, pp.1-537, 2016.
[24] S. Niu et al., "Theoretical study of contact-mode triboelectric nanogenerators as an effective power source," *Energy Environ. Sci*, vol. 6, no. 12, pp. 3576-3583, 2013.
[25] Y. Zhou et al., "Manipulating Nanoscale Contact Electrification by an Applied Electric Field", Nano Lett, vol. 14, no. 3, pp. 1567-1572, 2014.
[26] R.D.I.G. Dharmasena et al.,"Triboelectric nanogenerators: providing a fundamental framework," *Energy Environ. Sci*, vol. 10, no. 8, pp. 1801-1811, 2017.
[27] R. Feynman, R. Leighton and M. Sands, *The Feynman Lectures on Physics*, Vol. I. Boulder: Basic Books, 2011, pp.1-560.
[28] J. Lee, J. Lee and J. Baik, " The Progress of PVDF as a Functional Material for Triboelectric Nanogenerators and Self-Powered Sensors ", *Micromachines*, vol. 9, no. 10, p. 532, 2018.
[29] A. Hinckley et al., "Investigation of a Solution-Processable, Nonspecific Surface Modifier for Low Cost, High Work Function Electrodes", *ACS Appl. Mater. Interfaces*, vol. 8, no. 30, pp. 19658-19664, 2016.
[30] J. Lee et al., "Robust nanogenerators based on graft copolymers via control of dielectrics for remarkable output power enhancement", *Sci. Adv*, vol. 3, no. 5, p. e1602902, 2017.
[31] P. Bai et al., "Dipole-moment-induced effect on contact electrification for triboelectric nanogenerators", *Nano Res*, vol. 7, no. 7, pp. 990-997, 2014.
[32] Y. Zi, H. Guo, Z. Wen, M. Yeh, C. Hu and Z. Wang, "Harvesting Low-Frequency (<5 Hz) Irregular Mechanical Energy: A Possible Killer Application of Triboelectric Nanogenerator", *ACS Nano*, vol. 10, no. 4, pp. 4797-4805, 2016.
[33] P. Vasandani, Z.-H. Mao, W. Jia, and M. Sun, "Relationship between triboelectric charge and contact force for two triboelectric layers,"J. Electrost, vol. 90, pp. 147-152, 2017.
[34] X. S. Zhang, M. Han, B. Kim, J.-F. Bao, J. Brugger and H. Zhang,"All-in-One Self-Powered Flexible Microsystems Based on Triboelectric Nanogenerators," *Nano Energy*, 2018.
[35] M. Parvez Mahmud, N. Huda, S. H. Farjana, M. Asadnia, and C. Lang, "Recent Advances in Nanogenerator - Driven Self - Powered Implantable Biomedical Devices," *Adv. Energy Mater*, vol. 8, no. 2, p. 1701210, 2018.
[36] G. Min, L. Manjakkal, D. M. Mulvihill, R. Dahiya, "Enhanced triboelectric nanogenerator performance via an optimised low permittivity, low thickness substrate," in *Proc. IEEE Sensors 2018*, Oct 2018, N. Delhi, India.
[37] S. Torabi et al., "Rough Electrode Creates Excess Capacitance in Thin-Film Capacitors", *ACS Appl. Mater. Interfaces*, vol. 9, no. 32, pp. 27290-27297, 2017.
[38] R. Dharmasena, K. Jayawardena, C. Mills, R. Dorey, and S. Silva, "A unified theoretical model for Triboelectric Nanogenerators," *Nano Energy*, vol. 48, pp. 391-400, 2018.
[39] J. Walker, Halliday & Resnick, *fundamentals of physics*. Hoboken: Wiley, pp. 1-1450, 2014.

Guanbo Min received a B.Sc. degree in Electronic Information Technology from Macau University of Science and Technology, Macao S.A.R, China in 2015 and a M.Sc. degree in Electronics and Electrical Engineering from University of Glasgow, UK in 2017. Since 2017, he has been a Ph.D. student at University of Glasgow. His work is focused on optimizing triboelectric nanogenerator performance and its applications in energy autonomous electronic skin.

Libu Manjakkal received B.Sc. and M.Sc. degrees in physics from Calicut University, and Mahatma Gandhi University, India. He received a Ph.D. degree in Electronic Engineering from Institute of Electron Technology (ITE), Poland (2012–2015). From 2009–2012 he worked at CMET, India. In 2012, he moved to New University of Lisbon, Portugal. From 2015–2016, he was a post-doctoral researcher with ITE. Since 2016, he has been a Research Associate at University of Glasgow. He has authored/co-authored 45 scientific papers. His research interests include material synthesis, electrochemical sensors, supercapacitors, flexible electronics and wearable systems.

Daniel Mulvihill is Lecturer in Mechanical Engineering at the University of Glasgow. He completed a D.Phil. in Engineering Science at the University of Oxford in 2012 and subsequently undertook postdoctoral periods at the University of Limerick, EPFL Switzerland and the University of Cambridge prior to joining Glasgow in 2016. His interests are mainly focused on materials engineering and tribology. Dr Mulvihill is a former Institution of Mechanical Engineers (IMechE) Tribology Trust Bronze Medalist (2013).

Ravinder Dahiya (S'05, M'09, SM'12) is Professor of Electronics and Nanoengineering in the University of Glasgow, U.K. He is the leader of Bendable Electronics and Sensing Technologies (BEST) research group, which conducts fundamental and applied research in the multidisciplinary fields of flexible and printable electronics, tactile sensing, electronic skin, robotics and wearable systems. He has authored over 250 research articles, 2 books, 2 monographs, 12 patents (including 7 submitted) and several book chapters. He has led several international projects on e-skin, tactile sensing, robotic skin and flexible electronics. He is a Distinguished Lecturer of the IEEE Sensors Council and is serving on the editorial boards of the Scientific Report and IEEE SENSORS JOURNAL. He was the TPC Chair of IEEE Sensors 2017 and IEEE Sensors 2018. He holds the prestigious EPSRC Fellowship and received in past the Marie Curie Fellowship and Japanese Monbusho Fellowship. Among several awards he has received, the most recent are 2016 Microelectronic Engineering Young Investigator Award and the 2016 Technical Achievement Award from the IEEE Sensors Council.